Supporting Information for

Original article

Targeting metabolic vulnerability in mitochondria conquers MEK inhibitor resistance in *KRAS*-mutant lung cancer

Juanjuan Feng[a,b,†], Zhengke Lian[a,†], Xinting Xia[a], Yue Lu[a], Kewen Hu[c], Yunpeng Zhang[a], Yanan Liu[a], Longmiao Hu[a], Kun Yuan[a], Zhenliang Sun[b,*], Xiufeng Pang[a,*]

[a]Shanghai Key Laboratory of Regulatory Biology, School of Life Sciences, East China Normal University, Shanghai 200241, China

[b]Joint Center for Translational Medicine, Southern Medical University Affiliated Fengxian Hospital, Shanghai 201499, China

[c]Cancer Institute, Fudan University Shanghai Cancer Center, Department of Oncology, Shanghai Medical College, Fudan University, Shanghai 200032, China

Received ; received in revised form; accepted

*Corresponding authors. Tel.: +86 21 24206942, +86 21 57416150.

E-mail addresses: xfpang@bio.ecnu.edu.cn (Xiufeng Pang), zhenliang@smu.edu.cn (Zhenliang Sun).

[†]These authors made equal contributions to this work.

1. Supporting figures S1–S9

2. Supporting tables S1–S5

1. Supporting figures

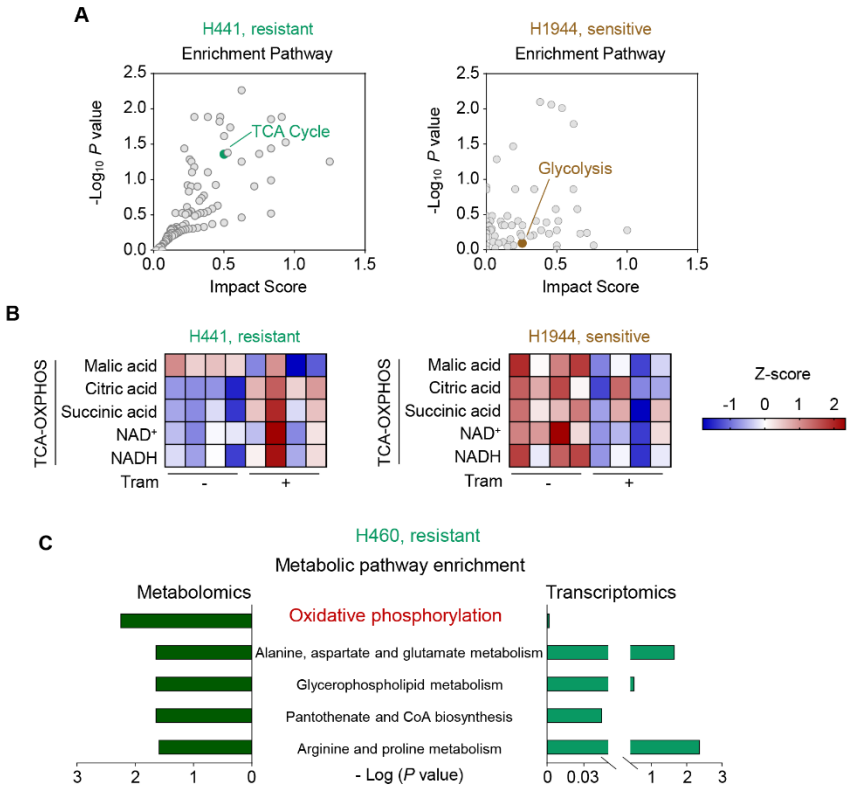

Figure S1. MEK inhibition activates mitochondrial oxidative metabolism. (A) Metabolites enrichment analysis. H441 and H1944 cells were treated with trametinib at their respective 1/2 IC_{50} values for 24 h and then harvested for metabolomic profiling determination. Metabolite set enrichment analysis was performed to identify dysregulated metabolic pathways (n = 4). (B) Abundance of major metabolites in the tricarboxylic acid (TCA)-oxidative phosphorylation (OXPHOS) pathway in trametinib-treated cells versus untreated cells. Metabolite abundance was normalized by cell number. NADH, nicotinamide adenine dinucleotide; NAD^+, oxidized nicotinamide adenine dinucleotide. Values are scaled as indicated (2 to −1). (C) The top 5 altered metabolic pathways in trametinib-treated H460 cells as compared with untreated control. H460 cells were treated with trametinib at their respective 1/2 IC_{50} for 24 h. Cells were then harvested and subjected to metabolomics (n = 6) and RNA sequencing (n = 3), respectively. The differential metabolites and genes enriched in KEGG biological pathway were analyzed.

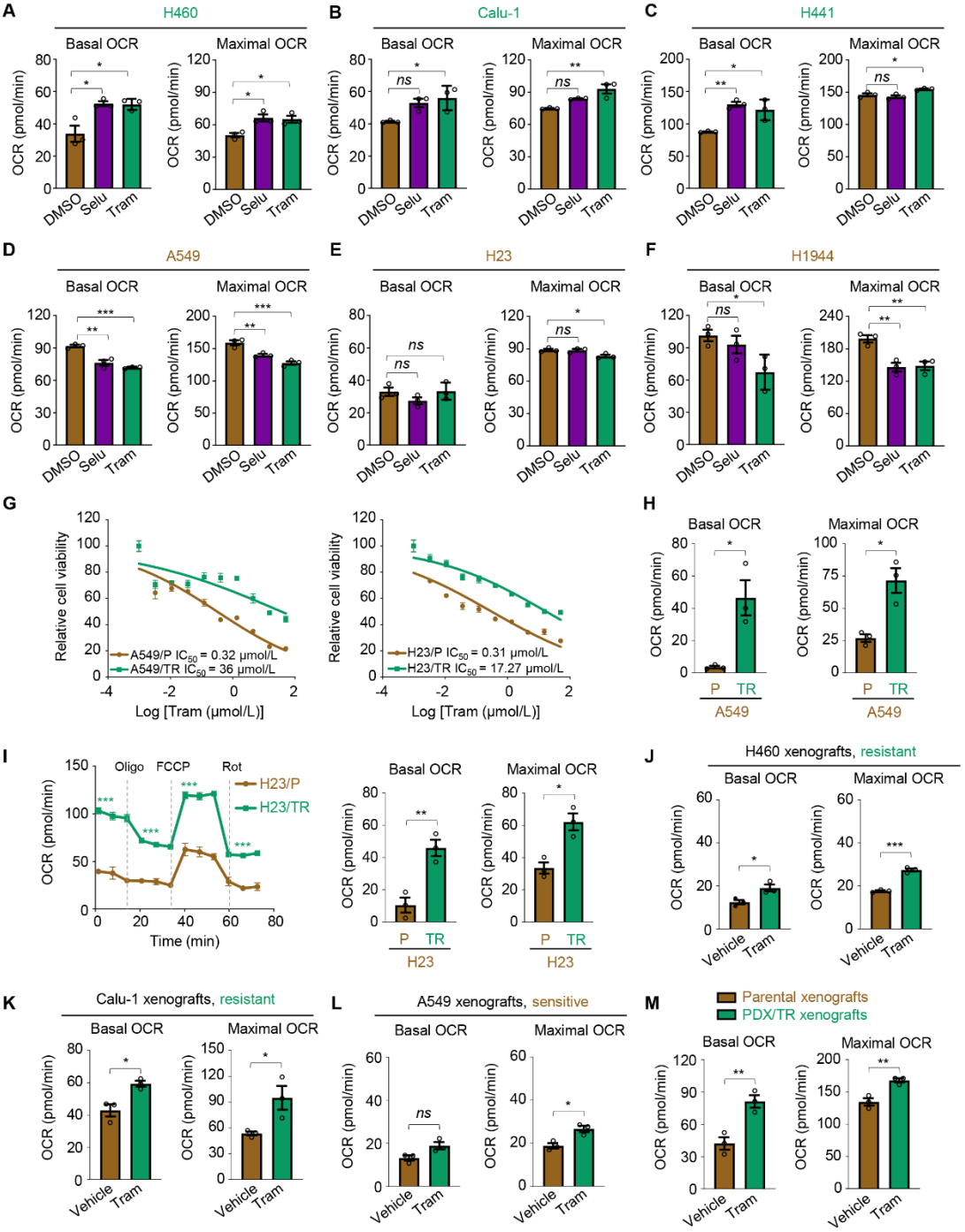

Figure S2. MEK inhibition favors oxidative energy metabolism in resistant cells and xenograft tumors. (A–F) The level of basal OCR and maximal OCR in NSCLC cells after MEKi treatment. MEKi-resistant cells (H460, Calu-1, and H441) (A–C) and MEKi-sensitive cells (A549, H23, and H1944) (D–F) were exposed to trametinib and selumetinib at their respective 1/2 IC_{50} values for 6 h. Basal OCR and maximal OCR were interpolated from the time course plot. Data represent the mean ± SEM of three technical replicates, representative of three independent experiments with similar results. *$P < 0.05$, **$P < 0.01$, and ***$P < 0.001$; *ns*, not significant, by one-way ANOVA

with Tukey's multiple-comparisons test. (G) Inhibitory effects of trametinib on acquired resistant cells (A549/TR or H23/TR) and their parental cells (A549/P or H23/P). Cells were treated with trametinib for 72 h, and cell viability was measured. Data represent the mean ± SEM of three technical replicates, representative of three independent experiments with similar results. (H) Basal OCR and maximal OCR in A549/TR cells and A549/P cells. Data represent the mean ± SEM of three technical replicates, representative of three independent experiments with similar results. *P < 0.05, by unpaired, two-sided Student's t test. (I) OCR in H23/TR cells and H23/P cells. A representative trace of OCR from a mitochondrial stress test is shown (*left*). Basal OCR and maximal OCR were calculated (*right*). Data represent the mean ± SEM of three technical replicates, representative of three independent experiments with similar results. *P < 0.05, **P < 0.01, and ***P < 0.001, by unpaired, two-sided Student's t test. (J–L) Basal OCR and maximal OCR in trametinib-treated and vehicle-treated tumors. Values are expressed as the mean ± SEM of three independent biologically samples. *P < 0.05, and ***P < 0.001; *ns*, not significant, by unpaired, two-sided Student's t test. (M) Basal OCR and maximal OCR in PDX/TR and parental xenografts. Values are expressed as the mean ± SEM of three independent biologically samples. **P < 0.01, by unpaired, two-sided Student's t test.

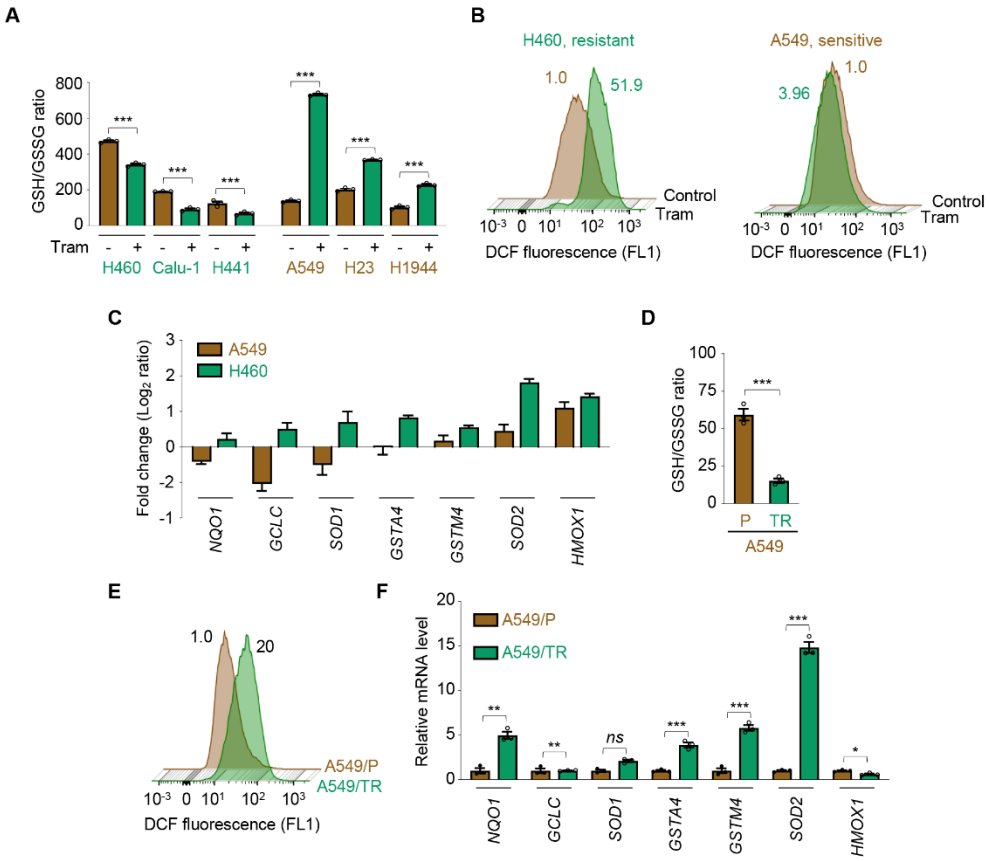

Figure S3. MEK inhibition increases redox stress in MEKi-resistant cells. (A) GSH/GSSG ratio in trametinib-treated NSCLC cells. MEKi-resistant cells (H460, Calu-1, and H441) and MEKi-sensitive cells (A549, H23, and H1944) were exposed to trametinib at their respective 1/2 IC_{50} values for 6 h. Cell lysates were subjected to glutathione (GSH) and L-glutathione oxidized (GSSG) measurement using a commercial kit. Data of GSH/GSSG ratio represent the mean ± SEM of biological triplicates. ***$P < 0.001$, by unpaired, two-sided Student's *t* test. (B) 3D plot showing ROS production. H460 and A549 cells were treated with trametinib for 6 h. The relative ROS production was calculated by setting the control group as 1. (C) Log_2 ratio values of fold change for *NQO1*, *GCLC*, *SOD1*, *GSTA4*, *GSTM4*, *SOD2*, and *HMOX1* transcripts in A549 and H460 cells before and after trametinib treatment. Cells were treated with trametinib at their respective 1/2 IC_{50} values for 24 h. qPCR analysis was further conducted. (D) GSH/GSSG ratio in A549/TR and their parental cells. Data represent the mean ± SEM of biological triplicates. ***$P < 0.001$, by unpaired, two-sided Student's *t* test. (E) ROS production of A549/TR and A549/P cells. (F) mRNA expression levels of *NQO1*, *GCLC*, *SOD1*, *GSTA4*, *GSTM4*, *SOD2*, and *HMOX1* in A549/TR and A549/P cells. Data represent the mean ± SEM of biological triplicates. *$P < 0.05$, **$P < 0.01$, and ***$P < 0.001$; *ns,* not significant, by unpaired, two-sided Student's *t* test.

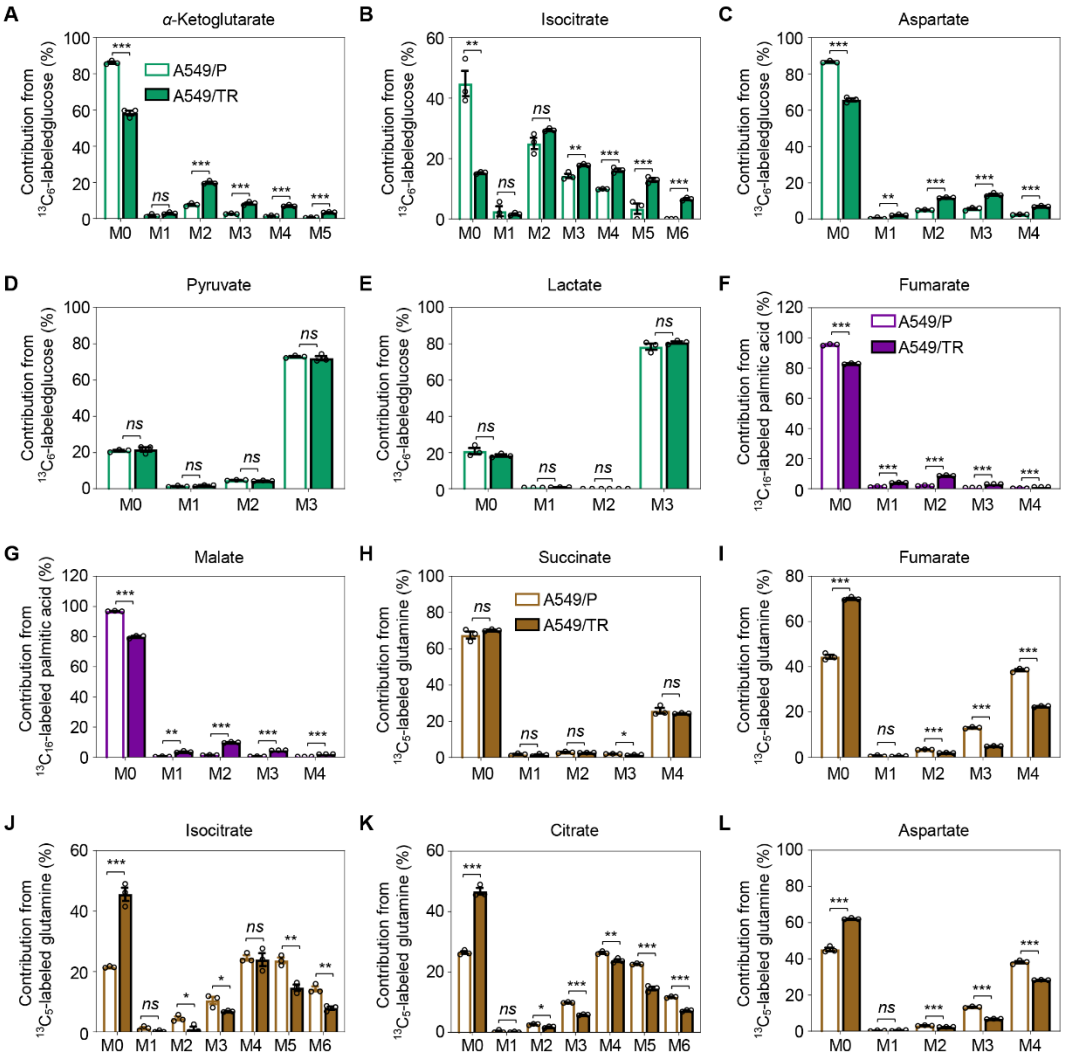

Figure S4. MEK inhibition favors enhanced carbon incorporation in TCA cycle metabolites. [U-$^{13}C_6$]-glucose (green), [U-$^{13}C_{16}$]-palmitate (purple) and [U-$^{13}C_5$]-glutamine (brown) tracing experiments in A549/P and A549/TR cells. Cells were cultured in the presence of [U-$^{13}C_6$]-glucose (12 h) (A–E), [U-$^{13}C_{16}$]-palmitate (12 h) (F, G), or [U-$^{13}C_5$]-glutamine (1 h) (H–L) prior to GC–MS analysis. The relative percentage of the isotopologues for each metabolite is shown. All data represent the mean ± SEM of biological triplicates. *$P < 0.05$, **$P < 0.01$, and ***$P < 0.001$; *ns,* not significant, by unpaired, two-sided Student's *t* test.

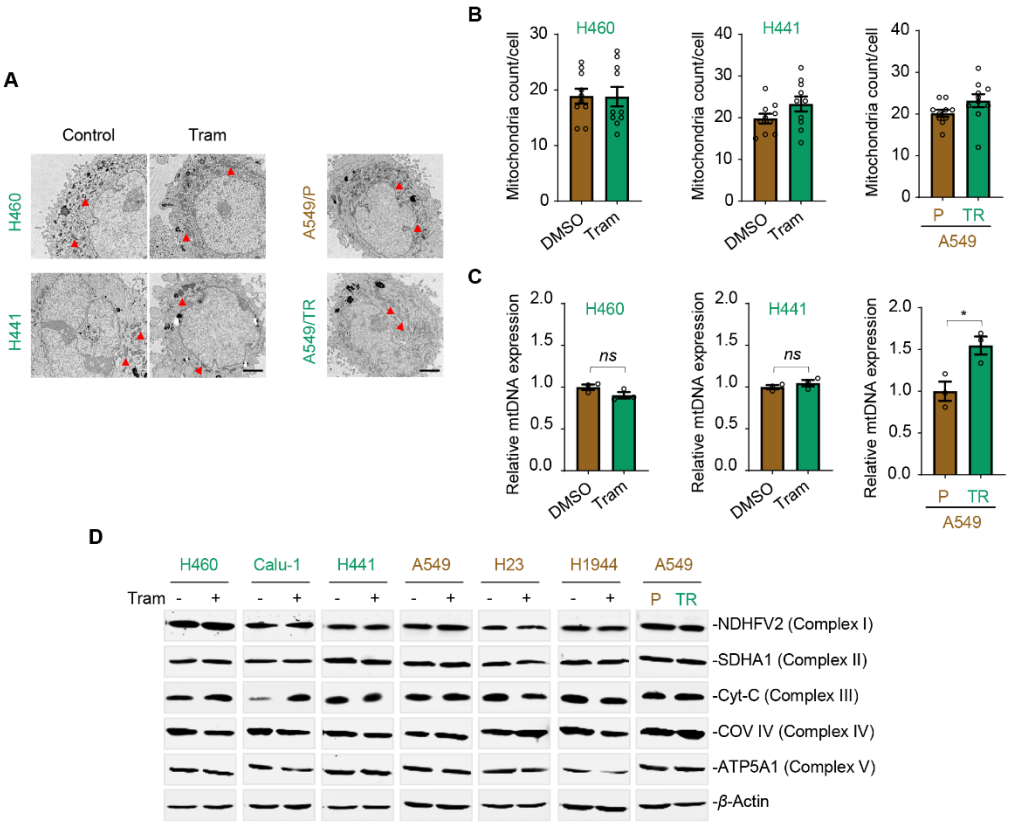

Figure S5. MEKi-resistance is not associated with mitochondrial function. (A) Mitochondria morphology of *KRAS*-mutant NSCLC cells. H460 and H441 cells were exposed to trametinib at their respective 1/2 IC_{50} values for 24 h. Mitochondrial morphology was detected by a HT7700 transmission electron microscope. Representative images from each group are shown. Red arrowheads indicate swelling of mitochondria. Scale bar, 2 μm. (B) Average mitochondria number. Mitochondria in 10 cells was counted. Data are shown as means ± SEM of biological triplicates. (C) Mitochondrial DNA copy number. H460 and H441 cells were treated with trametinib at their respective 1/2 IC_{50} values for 24 h. Nuclear and mitochondrial DNA content was measured using qPCR. Mitochondrial DNA content was determined by normalizing mitochondrial DNA abundance [tRNA-Leu (UUR)] to nuclear DNA (β2M) abundance. Data represent the mean ± SEM of biological triplicates. *ns*, not significant, by unpaired, two-sided Student's *t* test. (D) Effects of trametinib on electron transport chain complex components. Cells were treated with trametinib at their respective 1/2 IC_{50} values for 24 h. Treated cells were collected and probed with antibodies against NDHFV2, SDHA1, Cyt-C, COV IV, and ATP5A1, respectively. Trametinib-resistant cell lines are marked in green, and trametinib-sensitive cell lines are marked in brown. Images are representative of three independent experiments with similar results.

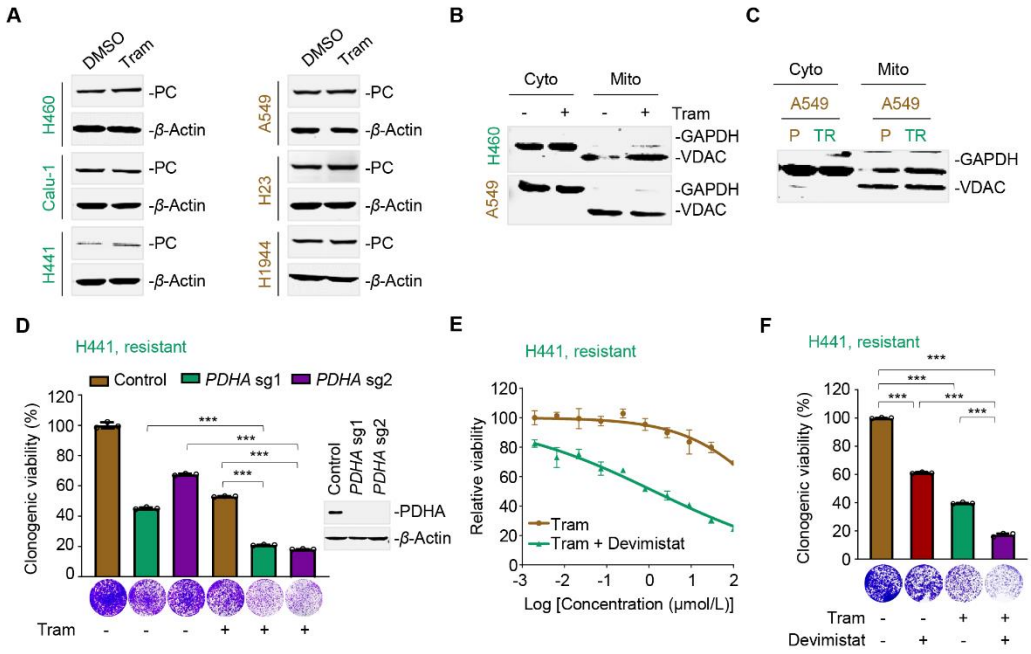

Figure S6. Intervention of PDHc sensitizes resistant cells to trametinib. (A) Pyruvate carboxylase (PC) protein levels. Cells were treated with trametinib at their respective 1/2 IC_{50} values for 24 h. PC expression was detected by immunoblot analysis. MEKi-resistant cell lines are marked in green and MEKi-sensitive cell lines are marked in brown. (B) Mitochondria fraction. H460 and A549 cells were exposed to trametinib for 24 h. Mitochondria was isolated by a mitochondria isolation kit. GAPDH and VDAC served as the cytoplasmic and mitochondrial fraction markers. (C) Mitochondria fraction in A549/P and A549/TR cells. (D) *PDHA* knockout synergized with trametinib in H441 cells. *Left*, relative viability of the culture colonies; *right*, *PDHA* knockout efficiency in H441 cells by immunoblot analysis. Data are shown as the mean ± SEM of biological triplicates. ***$P < 0.001$, by one-way ANOVA with Tukey's multiple-comparisons test. (E, F) PDHc inhibition by devimistat re-sensitized the inhibitory effects of trametinib on H441 cells. Growth curves (E) and the relative viability of cultured colonies (F) are shown. Data are shown as the mean ± SEM of biological triplicates. ***$P < 0.001$, by one-way ANOVA with Tukey's multiple-comparisons test.

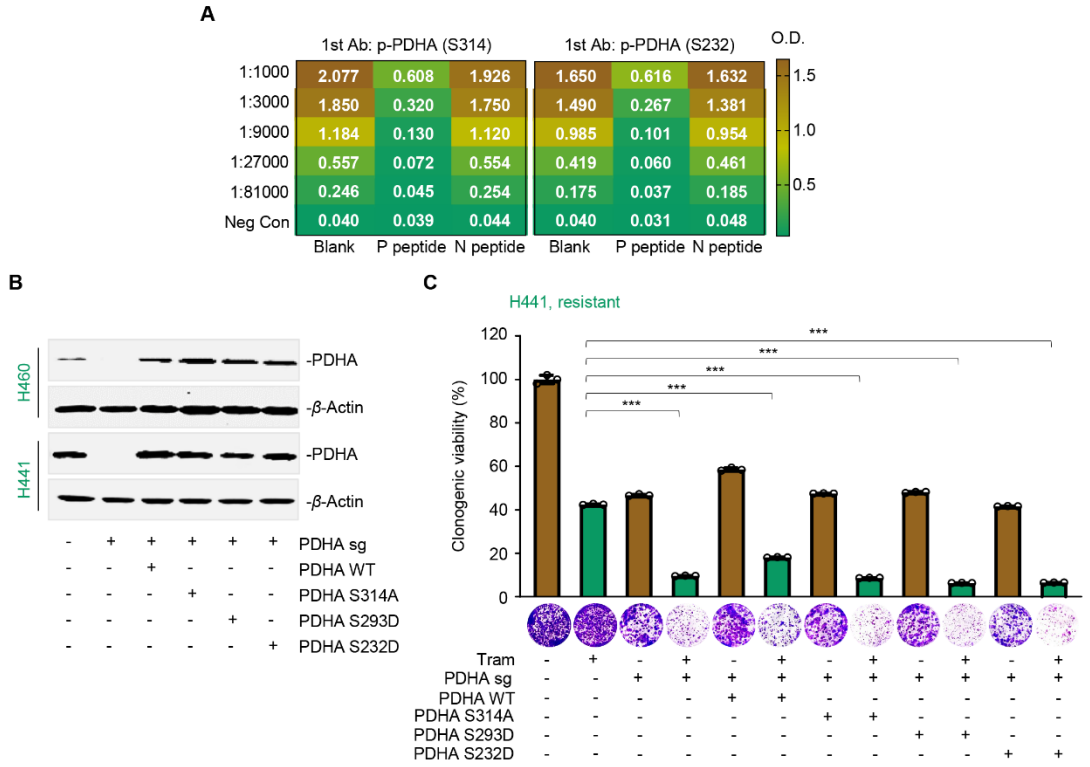

Figure S7. PDHA phosphorylation maintains PDHc activity. (A) Enzyme-linked immunosorbent assays. Series diluted p-PDHA (S314) and p-PDHA (S232) antibodies were used to detect P peptide and N peptide. P peptide, phospho-peptide; N peptide, non-phospho-peptide. (B) *PDHA* knockout and reconstitution of PDHA WT, PDHA S314A, PDHA S293D, and PDHA S232D in H460 and H441 cells. PDHA protein abundance was detected by immunoblot analysis. (C) Colony formation assays. H441 cells were depleted of endogenous PDHA, followed by reconstitution of PDH WT, PDH S314A, PDH S293D, and PDH S232D. Transfected H441 cells were then treated with or without trametinib for 7–10 days. Clonogenic assays were carried out. Data are presented as the mean ± SEM of three independent experiments. *** $P < 0.001$, by unpaired, two-sided Student's *t* test.

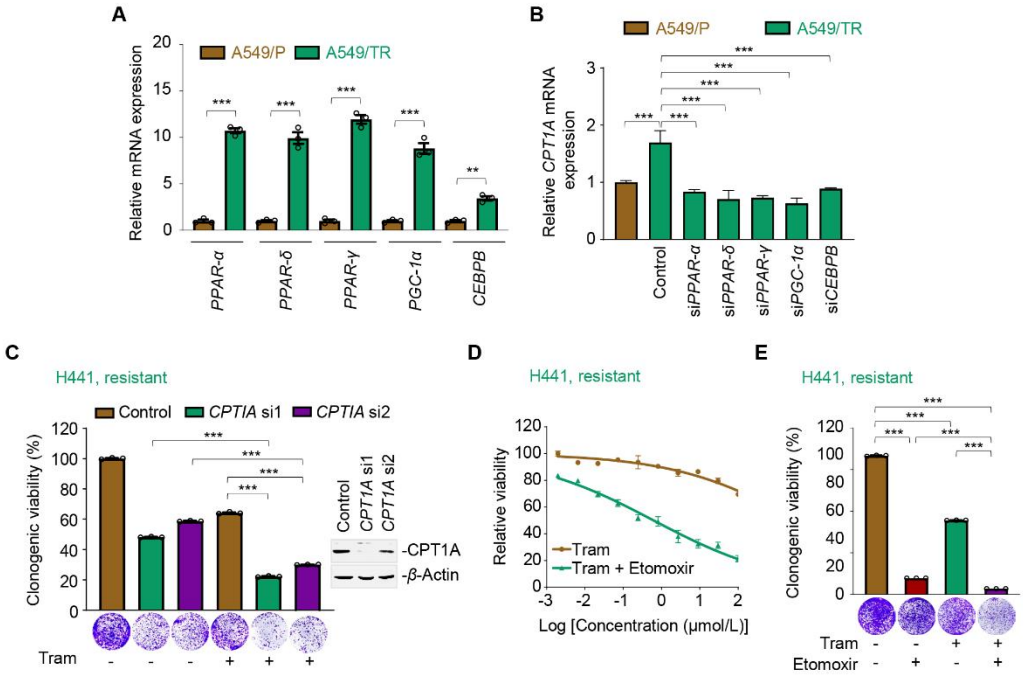

Figure S8. CPTIA is required for the therapeutic efficacy of trametinib. (A) Relative mRNA expression levels of *PPARα*, *PPARδ*, *PPARγ*, *PGC-1α*, and *CEBPB* in A549/TR cells and their parental cells. Data represent the mean ± SEM of biological triplicates. $^{**}P < 0.01$, and $^{***}P < 0.001$, by unpaired, two-sided Student's *t* test. (B) CPTIA expression in A549/TR cells after *PPARs*, *PGC-1α*, or *CEBPB* genetical silencing. (C) *CPTIA* silencing increased the sensitivity of H441 to trametinib. *Left*, relative viability of the cultured colonies; *right*, efficacy of *CPTIA* knockdown by immunoblot analysis. Data represent the mean ± SEM of biological triplicates. $^{***}P < 0.001$, by one-way ANOVA with Tukey's multiple-comparisons test. (D, E) Etomoxir enhanced the killing efficacy of trametinib in H441 cells. Growth curves (D) and the relative viability of cultured colonies (E) are shown. Data represent the mean ± SEM of biological triplicates. $^{***}P < 0.001$, by one-way ANOVA with Tukey's multiple-comparisons test.

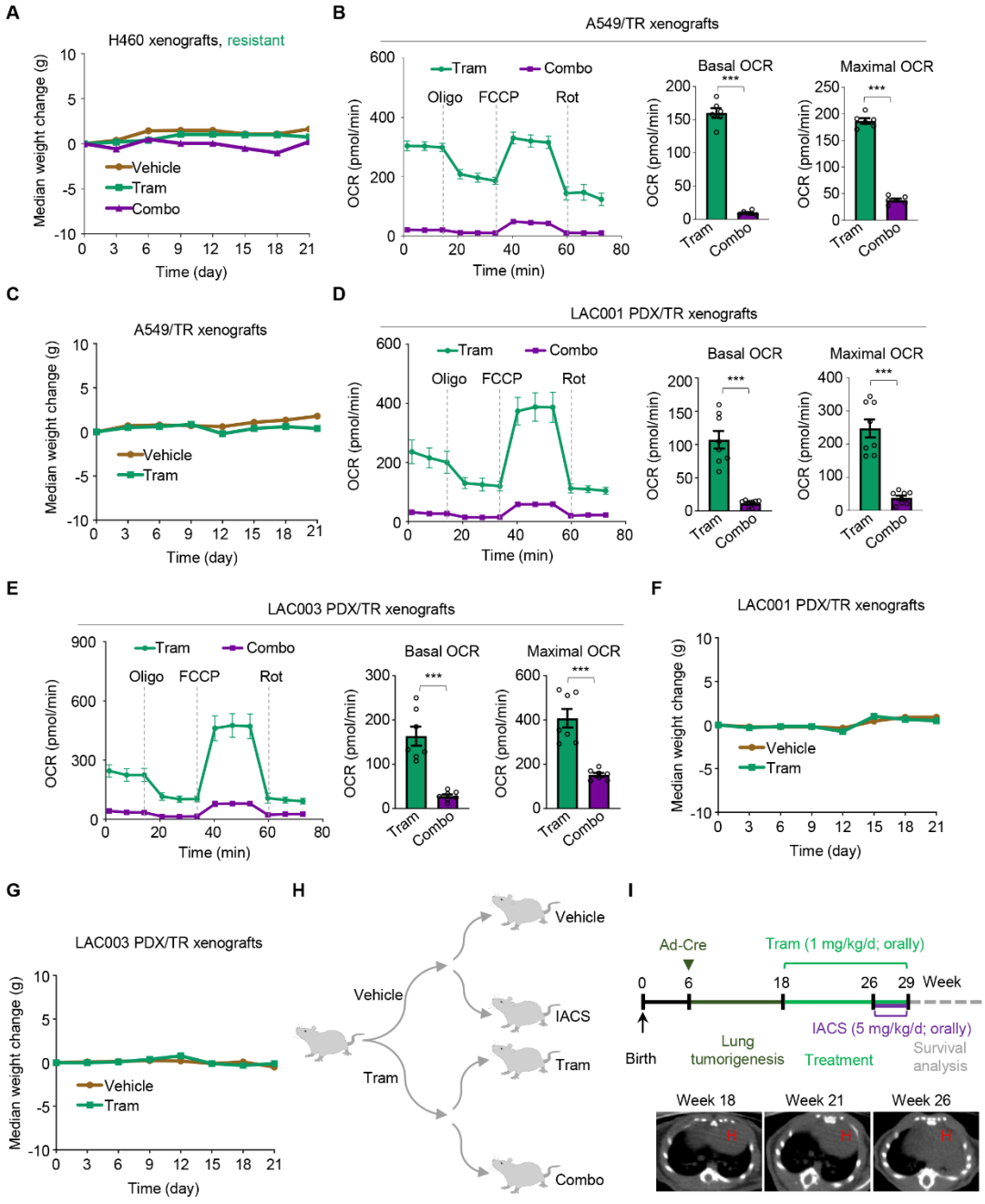

Figure S9. *In vivo* efficacy of trametinib and IACS-010759 combination. (A) The mouse body weight on Day 21 (n = 6 per group). Data represent the mean ± SEM. (B) OCR levels in combo-treated and trametinib-treated A549/TR xenograft tumors. The representative trace of OCR values from a mitochondrial stress test is shown (*left*). Basal OCR and maximal OCR were interpolated from the time course plot (*right*). Values are expressed as the mean ± SEM of three independent biologically samples. ***P < 0.001, by unpaired, two-sided Student's t test. (C) The mouse body weight on day 21 (n = 6 per group). Data are presented as the mean ± SEM. (D, E) OCR levels in

combo-treated and trametinib-treated LAC001 and LAC003 PDX/TR xenograft tumors. A representative trace of OCR values from a mitochondrial stress test is shown (*left*). Basal OCR and maximal OCR were interpolated from the time course plot (*right*). Values are expressed as the mean ± SEM of three independent biologically samples. ***$P < 0.001$, by unpaired, two-sided Student's *t* test. (F, G) Mouse body weight of LAC001 (F; $n = 8$ per group) and LAC003 PDX/TR bearing mice (G; $n = 7$ per group). Values are the mean ± SEM. (H) Treatment scheme. (I) schematic diagram showing the generation of LSL-*Kras*$^{G12D/+}$; *Trp53*$^{fl/fl}$ mouse model (KP) with trametinib-resistant tumors. H, heart.

2. Supporting tables

Table S1 KRAS mutant status of the cell lines employed.

Histology	Cell lines	KRAS mutation	Medium	RRID
Lung, adenocarcinoma	H460	Q61H	RMPI1640	CVCL_0459
	Calu-1	G12C	DMEM	CVCL_0608
	H441	G12V	RMPI1640	CVCL_1561
	H292	G12S	RMPI1640	CVCL_0455
	A549	G12S	RMPI1640	CVCL_0023
	H23	G12C	RMPI1640	CVCL_1547
	H1944	G13D	RMPI1640	CVCL_1508
	H358	G12C	RMPI1640	CVCL_1559

Table S2 Primers for RT-qPCR assays.

RT-qPCR primer sequences	
Primer lables	Sequences
CPTIA #F	TGCCCTGAGACGGGGATTAT
CPTIA #R	TTTCCAGCCCAGCACATGAA
NQO1 #F	CAGCTCACCGAGAGCCTAGT
NQO1 #R	GAGTGAGCCAGTACGATCAGTG
GCLC #F	ATGCCATGGGATTTGGAAT
GCLC #R	AGATATACTGCAGGCTTGGAATG
SOD1 #F	TCATCAATTTCGAGCAGAAGG
SOD1 #R	CAGGCCTTCAGTCAGTCCTTT
GSTA4 #F	AGTTGTACAAGTTGCAGGATGG
GSTA4 #R	CAATTTCAACCATGGGCACT
GSTM4 #F	TCATCTCCCGCTTTGAGG
GSTM4 #R	CAGACAGCCACCCTTGTGTA
SOD2 #F	CTGGACAAACCTCAGCCCTA
SOD2 #R	TGATGGCTTCCAGCAACTC
HMOX1 #F	GGGTGATAGAAGAGGCCAAGA
HMOX1 #R	AGCTCCTGCAACTCCTCAAA
PPARα #F	GAAGCTGTCACCACAGTAGC
PPARα #R	TTCCAGAACTATCCTCGCCG
PPARδ #F	AGTGTTGTACAGTGTTTTGGGC
PPARδ #R	AGACCATTCCAGACCCTCGT
PPARγ #F	GTGACCAGAAGCCTGCATTT
PPARγ #R	GTCAACCATGGTCATTTCGTT
PGC-1α #F	GTAAATCTGCGGGATGATGG
PGC-1α #R	AATTGCTTGCGTCCACAAA
CEBPB #F	AGAGGCGTCTGTATATTTTGGG
CEBPB #R	TGCCCCCAAAAGGCTTTGTAA
β2m #F	TGCTGTCTCCATGTTTGATGTATCT
β2m #R	TCTCTGCTCCCCACCTCTAAGT
tRNA-Leu(UUR) #F	CACCCAAGAACAGGGTTTGT
tRNA-Leu(UUR) #R	TGGCCATGGGTATGTTGTTA
β-Actin #F	GGGACCTGACTGACTACCTC
β-Actin #R	ATCTTCATTGTGCTGGGTG

siRNA sequences		
Target genes	Sequences	
human *CPTIA* si1	AGAAGUUCAUCAGAUUCAAGA	
human *CPTIA* si2	UUGUCUAAGAGCUUCAUGGCU	
CRISPR gRNA sequences		
Target genes	Sequences	Target location
human *PDHA* sg1	AGAAGCGCCAGACAGCACGC	exon 1
human *PDHA* sg2	GGCCTTCTTCCAGCCGGTGA	exon 3

Table S3 Antibodies used for immunoblotting and immunoprecipitation.

Protein target	Company	Catalog Number	Dilution	RRID
PDHA	Abcam	ab110330	1:1000	AB_10858459
p-PDHA S293	Abcam	ab177461	1:1000	AB_2756339
NDUFV2	Abcam	ab96117	1:1000	AB_10678713
ATP5A1	Abclonal	A5884	1:1000	AB_2766632
PDHK1	Abclonal	A0834	1:1000	AB_2757420
PDP2	Abclonal	A14416	1:1000	AB_2761285
CPTIA	Abclonal	A5307	1:1000	AB_2766119
COX IV	CST	#4850	1:1000	AB_2085424
Cyt-C	CST	#11940	1:1000	AB_2637071
SDHA1	CST	#11998	1:1000	AB_2750900
VDAC	CST	#4866	1:1000	AB_2272627
GAPDH	CST	#5174	1:10000	AB_10622025
β-Actin	Abways Technology	AB0035	1:10000	AB_2904142
p-PDHA S232	Shanghai Genomics	/	1:1000	/
p-PDHA S314	Shanghai Genomics	/	1:1000	/

Table S4 Metabolomic and transcriptomic analysis of enriched metabolic pathways after trametinib treatment.

Metabolomics pathway enrichment in H460 cells after trametinib treatment						
Pathway	Metabolomic			Transcriptomic		
	Total	Hits	Raw *p*	Total	Hits	Raw *p*
Oxidative phosphorylation	5	4	0.005568	123	35	0.999136
Alanine, aspartate and glutamate metabolism	4	4	0.022406	32	14	0.466658
Glycerophospholipid metabolism	4	4	0.022406	82	31	0.788956
Pantothenate and CoA biosynthesis	4	4	0.022406	15	3	0.979559
Arginine and proline metabolism	4	4	0.025211	46	21	0.336001
Vitamin digestion and absorption	4	3	0.025211	19	10	0.225627
Thiamine metabolism	4	3	0.039167	14	5	0.75939
Calcium signaling pathway	2	2	0.039167	152	47	0.997589
AMPK signaling pathway	2	2	0.039167	108	41	0.805057
Longevity regulating pathway	2	2	0.039167	76	32	0.504464
cAMP signaling pathway	2	2	0.058987	165	65	0.741086
Nicotinate and nicotinamide metabolism	2	2	0.094903	27	11	0.606327
Ascorbate and aldarate metabolism	3	3	0.102965	10	3	0.856593
Glutathione metabolism	6	3	0.102965	46	28	0.006217
Aldosterone synthesis and secretion	3	2	0.144213	83	31	0.813876
Galactose metabolism	3	2	0.153366	26	11	0.543365
Glyoxylate and dicarboxylate metabolism	7	5	0.153366	25	15	0.048194
Nitrogen metabolism	7	3	0.153366	14	4	0.89827
Sphingolipid signaling pathway	2	2	0.153366	111	47	0.468225
Thyroid hormone synthesis	2	2	0.153366	60	23	0.73711
Choline metabolism in cancer	2	2	0.153366	91	45	0.076337
Aminoacyl-tRNA biosynthesis	9	6	0.153664	41	19	0.31831
Cysteine and methionine metabolism	10	6	0.190938	44	24	0.055433
Mannose type O-glycan biosynthesis	1	1	0.20202	23	7	0.90446
Sphingolipid metabolism	1	1	0.20202	42	19	0.367927
HIF-1 signaling pathway	1	1	0.20202	92	38	0.55895
Phosphatidylinositol signaling system	1	1	0.20202	90	34	0.798703
Pancreatic secretion	1	1	0.20202	69	27	0.700977
Neuroactive ligand-receptor interaction	6	1	0.211427	171	40	1
Ferroptosis	4	3	0.299625	39	25	0.003636
Central carbon metabolism in cancer	4	3	0.299625	57	24	0.516538
Protein digestion and absorption	9	5	0.315681	70	30	0.45684
Tryptophan metabolism	2	1	0.364873	33	13	0.662619
Inositol phosphate metabolism	2	1	0.364873	67	26	0.718183
Propanoate metabolism	2	1	0.364873	31	14	0.406732
Butanoate metabolism	2	1	0.364873	21	9	0.534558

Retrograde endocannabinoid signaling	2	1	0.364873	123	37	0.996978
Oxytocin signaling pathway	2	1	0.364873	135	50	0.878215
Salivary secretion	2	1	0.364873	64	26	0.606837
Arginine biosynthesis	5	3	0.381913	19	5	0.946929
beta-Alanine metabolism	5	3	0.381913	27	12	0.451784
Arachidonic acid metabolism	5	3	0.381913	42	15	0.822612
Mineral absorption	5	3	0.381913	40	20	0.176516
Glycolysis/Gluconeogenesis	1	1	0.393939	57	25	0.409865
Folate biosynthesis	1	1	0.393939	23	10	0.504569
Terpenoid backbone biosynthesis	5	1	0.393939	21	12	0.109851
Metabolism of xenobiotics by cytochrome P450	1	1	0.393939	42	15	0.822612
FoxO signaling pathway	1	1	0.393939	120	59	0.053518
mTOR signaling pathway	1	1	0.393939	137	65	0.092242
PI3K-Akt signaling pathway	1	1	0.393939	292	130	0.159347
Synaptic vesicle cycle	1	1	0.393939	50	20	0.640369
Glutamatergic synapse	1	1	0.393939	95	29	0.990295
Cholinergic synapse	1	1	0.393939	98	26	0.999371
GABAergic synapse	1	1	0.393939	69	23	0.936639
Regulation of actin cytoskeleton	1	1	0.393939	188	94	0.010646
Insulin secretion	1	1	0.393939	69	23	0.936639
Glucagon signaling pathway	1	1	0.393939	91	33	0.872859
Proximal tubule bicarbonate reclamation	1	1	0.393939	21	7	0.838007
Gastric acid secretion	1	1	0.393939	59	3	0.701431
Carbohydrate digestion and absorption	1	1	0.393939	29	8	0.960041
Morphine addiction	1	1	0.393939	69	30	0.416467
Nicotine addiction	1	1	0.393939	26	4	0.999054
African trypanosomiasis	1	1	0.393939	26	11	0.543365
Tyrosine metabolism	3	1	0.495827	25	6	0.979693
Phenylalanine metabolism	3	1	0.495827	14	3	0.969203
Starch and sucrose metabolism	3	1	0.495827	25	11	0.477084
Bile secretion	12	6	0.538554	51	24	0.253498
Carbon metabolism	3	2	0.561416	105	57	0.005324
Taste transduction	3	2	0.561416	41	11	0.983222
Regulation of lipolysis in adipocytes	3	2	0.561416	45	16	0.833957
Renin secretion	3	2	0.561416	55	25	0.323127
ABC transporters	6	2	0.597734	38	16	0.534104
Histidine metabolism	4	2	0.646413	20	9	0.460498
cGMP-PKG signaling pathway	4	2	0.646413	143	52	0.913714
Serotonergic synapse	4	2	0.646413	86	24	0.997057
Pyrimidine metabolism	6	3	0.679687	98	59	0.000134
Glycine, serine and threonine metabolism	6	3	0.679687	35	13	0.75691
Primary bile acid biosynthesis	4	1	1	12	5	0.605212
Pentose phosphate pathway	2	1	1	27	12	0.451784
Fructose and mannose metabolism	2	1	1	32	11	0.84266
Purine metabolism	14	6	1	159	83	0.003858
Linoleic acid metabolism	2	1	1	16	2	0.997726
Porphyrin and chlorophyll metabolism	2	1	1	25	12	0.322487
Drug metabolism-cytochrome P450	2	1	1	37	11	0.950895
Vascular smooth muscle contraction	2	1	1	99	35	0.914654
Alcoholism	2	1	1	148	47	0.994854

Table S5 Biochemistry testing of plasma from MEKi-resistant xenograft mice.

H460 xenograft mouse model			
Item	Group	Value	*P*-value (Treatment *vs*. Vehicle)
CR (μmol/L)	Vehicle	15.6 ± 2.9	
	Tram	11.8 ± 1.1	0.2616
	Combo	10.6 ± 1.6	0.1722
BUN (mmol/L)	Vehicle	8.2 ± 0.7	
	Tram	7.2 ± 0.3	0.1913
	Combo	11.0 ± 0.6	0.0118
AST (U/L)	Vehicle	197.6 ± 32.7	
	Tram	196.0 ± 19.5	0.9675
	Combo	247.0 ± 15.0	0.2069
ALT (U/L)	Vehicle	32.0 ± 3.6	
	Tram	32.4 ± 2.4	0.9294
	Combo	35.0 ± 5.8	0.5215
AST/ALT	Vehicle	6.3 ± 0.9	
	Tram	6.1 ± 0.4	0.8101
	Combo	7.1 ± 0.5	0.4321

A549/TR xenograft mouse model			
Item	Group	Value	*P*-value (Treatment *vs*. Vehicle)
CR (μmol/L)	Tram	15.4 ± 0.7	
	Combo	17.2 ± 1.3	0.2693
BUN (mmol/L)	Tram	8.3 ± 0.6	
	Combo	12.4 ± 0.6	0.0273
AST (U/L)	Tram	225.0 ± 16.2	
	Combo	198.8 ± 16.6	0.2918
ALT (U/L)	Tram	60.8 ± 5.5	
	Combo	50.2 ± 3.2	0.1351
AST/ALT	Tram	3.7 ± 0.2	
	Combo	4.1 ± 0.5	0.5570

LAC PDX/TR xenograft mouse model			
Item	Group	Value	*P*-value (Treatment *vs*. Vehicle)
CR (μmol/L)	Tram	27.4 ± 8.8	
	Combo	20.4 ± 4.2	0.4936
BUN (mmol/L)	Tram	10.3 ± 0.5	
	Combo	10.8 ± 0.6	0.0170
AST (U/L)	Tram	178.6 ± 11.3	
	Combo	227.4 ± 27.4	0.1379
ALT (U/L)	Tram	32.8 ± 4.0	
	Combo	37.2 ± 1.7	0.3360
AST/ALT	Tram	5.8 ± 0.9	
	Combo	6.2 ± 0.9	0.7698